



1 **GTDI: a gaming integrated drought index implying hazard**
2 **causing and bearing impacts changing**

3 Xiaowei Zhao¹, Tianzeng Yang¹, Hongbo Zhang^{1,2,3*}, Tian Lan¹, Chaowei Xue¹, Tongfang Li¹, Zhaoxia
4 Ye¹, Zhifang Yang¹, Yurou Zhang¹

5

6 ¹ School of Water and Environment, Chang'an University, Xi'an, 710054, China

7 ² Key Laboratory of Subsurface Hydrology and Ecological Effect in Arid Region of Ministry of

8 Education, Chang'an University, Xi'an, 710054, China

9 ³ Key Laboratory of Eco-hydrology and Water Security in Arid and Semi-arid Regions of the
10 Ministry of Water Resources, Chang'an University, Xi'an 710054, China

11

12 **Corresponding author:** hbzhang@chd.edu.cn

13

14 **Abstract:** Developing an effective and reliable integrated drought index is crucial for tracking and
15 identifying droughts. The study employs game theory to create a spatially variable weight drought
16 index (GTDI) by combining two single-type indices: the agricultural drought index (SSMI), which
17 implies drought hazard-bearing conditions, and the meteorological drought index (SPEI), which
18 implies drought hazard-causing conditions. Also, the entropy theory-based drought index (ETDI) is
19 induced to incorporate a spatial comparison to the GTDI to illustrate the rationality of gaming weight
20 integration. Leaf Area Index (LAI) data is employed to confirm the reliability of the GTDI in
21 identifying drought by comparing it with the SPEI, SSMI, and ETDI. Furthermore, an assessment



22 is conducted on the temporal trajectories and spatial evolution of the GTDI-identified drought to
23 discuss the GTDI's advancedness in monitoring changes in hazard-causing and bearing impacts.
24 The results showed that the GTDI has a greatly high correlation with single-type drought indices
25 (SPEI and SSMI), and its gaming weight integration is more logical and trustworthy than the ETDI.
26 As a result, it outperforms ETDI, SPEI, and SSMI in recognizing drought spatiotemporally, and is
27 projected to replace single-type drought indices to provide a more accurate picture of actual drought.
28 Additionally, GTDI exhibits the gaming feature, indicating a distinct benefit in monitoring changes
29 in hazard-causing and bearing impacts. The case studies show drought events in the Wei River Basin
30 are dominated by a lack of precipitation. The hazard-causing index SPEI dominates the early stages
31 of a drought event, whereas the hazard-bearing index SSMI dominates the later stages. This study
32 surely serves as a helpful reference for the development of integrated drought indices as well as
33 regional drought mitigation, prevention, and monitoring.

34 **Keywords:** Integrated drought index; GTDI; drought identification; LAI; Wei River Basin

35 **1 Introduction**

36 Drought is one of the most widespread and frequent natural hazards, commonly associated with
37 inadequate rainfall, a deficit in soil moisture, and reduced stream flow (Berg et al., 2018; Zhang et
38 al., 2022; AghaKouchak et al., 2023). Due to the combined pressures of climate change and human
39 activities, the intensity of global drought and the area of arid land have expanded dramatically since
40 the 21st century (Dai et al., 2013; Huang et al., 2016), severely constraining socio-economic
41 development and human livelihoods. Moreover, global warming is projected to increase the
42 frequency and severity of future drought occurrences (Trenberth et al., 2014; Vicente-Serrano et al.,



43 2020).

44 China, with its complex terrain and diverse climate types, is one of the countries suffering the
45 most severe drought-related losses worldwide (Dai et al., 2011; Zhang et al., 2021). Drought is
46 responsible for more than half of the economic losses caused by climatic hazards in China (Wang et
47 al., 2023). According to the Ministry of Water Resources of China (MWRC, 2022), the average
48 annual impacted area of crops and grain loss due to drought was 19.51 million hm^2 and 15.8 billion
49 kg, respectively, from 1950 to 2022. The loss has become increasingly severe, particularly after
50 2006, resulting in direct economic losses of more than US\$ 160 billion in China. For example, the
51 severe drought event that occurred in southern China from autumn 2009 to spring 2010 deprived
52 almost 21 million people of drinking water, with direct economic losses of nearly US\$3 billion
53 (Yang et al., 2012). Furthermore, the ongoing drought in China may worsen in the future (Leng et
54 al., 2015; Wang et al., 2018), with drought occurrences becoming more frequent, intense, and
55 extended. As a result, scientifically identifying regional drought risks and clarifying regional
56 drought development and evolution patterns can assist in actively developing drought mitigation
57 and disaster reduction strategies, assuring the security of food supply and water use.

58 Drought is currently categorized into four types based on distinct description objects:
59 meteorological, agricultural, hydrological, and socioeconomic droughts (Wilhite and Glantz, 1985;
60 Shah and Mishra, 2020). Meteorological drought is characterized by insufficient precipitation,
61 whereas agricultural drought occurs when soil moisture fails to meet crop development requirements.
62 Hydrological drought is primarily caused by a lack of surface runoff and groundwater (Xu et al.,
63 2019; Saha et al., 2023). Socioeconomic drought arises when the aforementioned causes disrupt the
64 human socioeconomic system, resulting in an imbalance between water supply and demand (Ding



65 et al., 2021). Despite differing definitions and emphasis, meteorological drought is always regarded
66 as the root cause of the other three types of drought (Ma et al., 2020). In terms of the driving
67 mechanism of drought occurrences, meteorological drought indicates the causative attribute of
68 drought (Zhang et al., 2023), whereas the other three primarily reflect the state of hazard-bearing
69 entities. Concurrently examining the hazard-causing and hazard-bearing components of drought is
70 essential for effective estimation and management of drought risk.

71 Drought is frequently identified using drought indices. The Standardized Precipitation Index
72 (SPI; Mckee et al., 1993) for meteorological drought, the Standardized Soil Moisture Index (SSMI;
73 Hao and AghaKouchak, 2013) for agricultural drought, and the Standardized Runoff Index (SRI;
74 Shukla and Wood, 2008) for hydrological drought are currently the most commonly used drought
75 indices. These single-type drought indices are primarily used for one-dimensional (type) drought
76 measurement & evaluation. However, due to the complexity and diversity of drought events, a
77 single-type drought index is unavoidably insufficient to handle the complete drought development
78 process (Chang et al., 2016; Wei et al., 2023). As a result, much effort has been expended in
79 developing comprehensive drought indices, such as the Palmer Drought Severity Index (PDSI;
80 Palmer, 1965). However, these indices are not very successful at distinguishing between
81 meteorological and agricultural drought influences and evaluating changes in regional patterns.
82 Because of this, some works refer to constructing a composite or integrated drought index in two or
83 more dimensions (Chang et al., 2016; Won et al., 2020; Wei et al., 2023), employing both linear and
84 nonlinear combination approaches.

85 The copula function is commonly employed in the nonlinear approach. Won et al. (2020)
86 proposed a copula-based joint drought index (CJDI) by combining the SPI and the evaporative



87 demand drought index (EDDI); Wei et al. (2023) used the copula function to connect precipitation,
88 NDVI, and runoff and then constructed the standardized comprehensive drought index (SCDI),
89 which has been applied to drought assessment in China's Yangtze River Basin. It should be noted
90 that copula functions are heavily reliant on the assumption that samples follow a specific probability
91 density function (Zhang et al., 2019). However, due to the complicated interactions between the
92 atmosphere, vegetation, soil, and groundwater, the drought does not generally meet it. If the copula
93 function is used to estimate drought quantiles, significant biases may be introduced, affecting the
94 reliability of the copula-based integrated drought indices (Huang et al., 2015).

95 A comprehensive drought index can also be generated by linearly mixing single-type drought
96 indices, such as the entropy weight method (Huang et al., 2015) and the principal component
97 analysis method (Liu et al., 2019). In the relevant research, it is highly emphasized that the weighting
98 of different types of drought indices is critical since it has a significant impact on the reliability of
99 drought monitoring results (Liu et al., 2019; Wei et al., 2023). Furthermore, it has been revealed that
100 the impacts of different factors on drought, such as hazard-causing and hazard-bearing, are changing
101 spatially and game-playing, necessitating the development of effective linear combination methods
102 for measuring their spatial heterogeneity in contribution to drought. Therefore, game theory is
103 suggested for the integration of drought indices because it can comprehensively consider the
104 opinions of each party to achieve a distribution pattern that satisfies each participant (Lai et al., 2015;
105 Jato-Espino and Ruiz-Puente, 2021), and has been widely applied in water resources management
106 (Madani, 2010; Khorshidi et al., 2019; Batabyal and Beladi, 2021).

107 This study proposes a game theory-based drought index (GTDI), which integrates the
108 meteorological drought index SPEI, implying hazard-causing impact, and the agricultural drought



109 index SSMI, implying hazard-bearing impact, through the game theory method. The structure of
110 this study is as follows: Section 2 introduces the research topic and data source. Section 3 describes
111 the SPEI, SSMI, GTDI, and ETDI (entropy theory-based drought index) calculation procedures, as
112 well as the verification and analysis methodologies. Section 4 investigates the evolutionary features
113 of GTDI, examines its rationality of integrated weight in comparison to ETDI, and validates its
114 usefulness in identifying drought occurrences using Leaf Area Index (LAI) data. Furthermore, the
115 impact of hazard-causing and bearing indices on GTDI's spatiotemporal evolution is explored
116 through the synergistic analysis of GTDI, SPEI, and SSMI. Finally, Section 5 highlights the study's
117 significant findings.

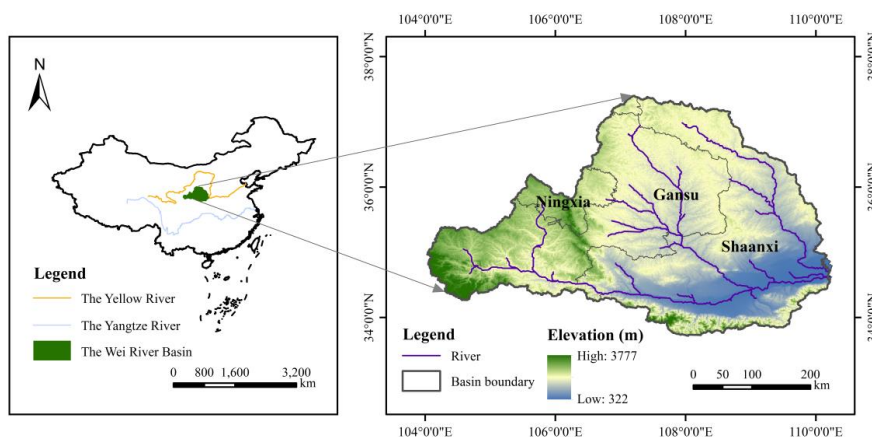
118 **2 Study area and data**

119 **2.1 Study area**

120 The Wei River is the largest tributary of the Yellow River, with a drainage area of 134,800 km² (Fig.
121 1). It rises to the north of Niaoshu Mountain in Gansu Province, about 33.5°–37.5°N latitude and
122 103.5°–110.5°E longitude, and runs primarily through Shaanxi, Gansu, and Ningxia provinces. The
123 Wei River Basin (WRB) is high in the west and low in the east, with a geographical elevation ranging
124 from 322 to 3777 meters. The WRB has a continental monsoon climate with large seasonal
125 fluctuations, with average annual temperatures and precipitation ranging from 7.8 to 13.5°C and
126 500 to 800 mm, respectively (Zhang et al., 2022). Precipitation in the WRB accounts for over 60%
127 of the total annual amount, and its spatial distribution shows a steady decrease from southeast to
128 northwest. Furthermore, evaporation is significant in the WRB, with annual water surface
129 evaporation ranging from 660 to 1600 mm. As a result of its specific climate characteristics, the



130 WRB is a typical place for drought research.



131

132 **Figure 1.** A map of the Wei River Basin.

133 2.2 Data source

134 The data used in this study comprises: (1) DEM data with a grid size of 30 m; (2) monthly
135 precipitation and temperature dataset from 1950 to 2020 with a grid size of 1 km; (3)
136 GLDAS_NOAH025_3H_2.0 and GLDAS_NOAH025_3H_2.1's soil moisture dataset for 0 to 10
137 cm of soil surface layer, with a spatial resolution of 0.25° and data period from 1950 to 2020; (4)
138 GLOBMAP leaf area index dataset (Version 3) with a period of 1981 to 2019 and a spatial resolution
139 of 0.08°. Additionally, in order to facilitate calculation and analysis, precipitation, air temperature,
140 soil moisture, and leaf area index (LAI) data were all resampled to the same spatial resolution of
141 0.125° in this study. The data source is shown in Table 1.

142 **Table 1.** Data source.

Name	Source
DEM data	http://www.ncdc.ac.cn/
Precipitation dataset	http://www.geodata.cn/
Temperature dataset	http://www.geodata.cn/
Soil moisture dataset	https://disc.gsfc.nasa.gov/datasets/



LAI dataset <https://www.resdc.cn/>

143 **3 Methodology**

144 **3.1 Calculation of single-type drought indices**

145 **3.1.1 SPEI**

146 The Standardized Precipitation Evapotranspiration Index (SPEI) was first introduced by Vicente
147 Serrano et al. in 2010. As a meteorological drought index, SPEI primarily characterizes the hazard-
148 causing attribute of drought (Zhang et al., 2023). On the basis of the Standardized Precipitation
149 Index (SPI), SPEI takes potential evapotranspiration (PET) into account and demonstrates superior
150 effectiveness and applicability (Labudová et al., 2017; Li et al., 2020; Tan et al., 2023). The
151 Thornthwaite method, which can better reflect the potential surface evapotranspiration, is employed
152 to calculate PET in this paper. As is well known, drought indices on different time scales can reflect
153 the dry and wet conditions of the study area during different periods. In this study, we calculated the
154 SPEI series over a three-month timescale. The detailed calculation procedure for SPEI can be found
155 in Vicente Serrano et al. (2010).

156 **3.1.2 SSMI**

157 Drought can have a direct impact on the growth state of hazard-bearing bodies such as crops (Zhang
158 et al., 2023), making agricultural drought hazard-bearing. The Standardized Soil Moisture Index
159 (SSMI) is one of the most effective indices for predicting agricultural drought (Hao et al., 2013),
160 and its calculation method is comparable to that of the SPI (Xu et al., 2021; You et al., 2022).
161 Meanwhile, it was revealed that the log-logistic probability distribution function with three
162 parameters was better suited to soil moisture data sequences than the original gamma probability



163 distribution function (Oertel et al., 2018). As a result, in this study, we employed the calculation
164 method proposed by Oertel et al. for the agricultural drought index SSMI, with a three-month time
165 scale, just like the SPEI.

166 **3.2 Construction of integrated drought indices**

167 In this study, two integrated drought indices, GTDI and ETDI, are built utilizing game theory and
168 the entropy weight method for index weight allocation, respectively, and both combine SPEI and
169 SSMI. ETDI serves as a comparison to GTDI, and Huang et al. (2015) provide the computation
170 process for it.

171 As a subset of optimality modeling, game theory (GT) investigates the interacting outcomes of
172 resource conflicts and cooperation between two or more entities (Lai et al., 2015). It attempts an
173 optimal allocation approach that maximizes the interests of each participant through mathematical
174 analysis (Jato-Espino and Ruiz-Puente, 2021). Currently, GT has been widely applied in the fields
175 of hydrology and water resources, such as water price equilibrium (Batabyal and Beladi, 2021),
176 reservoir scheduling policy (Khorshidi et al., 2019), and subjective/objective weighting issues (Liu
177 et al., 2020). In this study, the hazard-causing index (SPEI) and the hazard-bearing index (SSMI)
178 are regarded as two opponents in the game. Through confrontation, the GT technique gets the ideal
179 weight allocation for both sides and then uses this to produce the integrated drought index (GTDI)
180 at each grid point. The following are the methods for creating GTDI using game theory:

181 **Step 1:** A possible weight set is combined by SPEI and SSMI in the form of an arbitrary linear
182 combination as follows:

$$V = \alpha_{spei} V_{spei}^T + \alpha_{ssmi} V_{ssmi}^T, (\alpha_{spei}, \alpha_{ssmi} > 0) \quad (1)$$



183 Where V is a possible combined vector, V_{spei} & V_{ssmi} are the weight vectors of SPEI and SSMI, and
 184 α_{spei} & α_{ssmi} are the weight coefficients.

185 **Step 2:** Minimize the deviation between V and V_k using the following formula:

$$\text{Min} \|V - V_k\|_2, (k = spei, ssmi) \quad (2)$$

186 **Step 3:** According to the differentiation property of the matrix, transform formula (2) into a
 187 first-order system of linear equations:

$$\begin{bmatrix} V_{spei} V_{spei}^T & V_{spei} V_{ssmi}^T \\ V_{ssmi} V_{spei}^T & V_{ssmi} V_{ssmi}^T \end{bmatrix} \begin{bmatrix} \alpha_{spei} \\ \alpha_{ssmi} \end{bmatrix} = \begin{bmatrix} V_{spei} V_{spei}^T \\ V_{ssmi} V_{ssmi}^T \end{bmatrix} \quad (3)$$

188 **Step 4:** Solve the weight coefficients α_{spei} and α_{ssmi} in equation (3) and normalize them.

$$\begin{cases} \alpha_{spei}^* = \alpha_{spei} / (\alpha_{spei} + \alpha_{ssmi}) \\ \alpha_{ssmi}^* = \alpha_{ssmi} / (\alpha_{spei} + \alpha_{ssmi}) \end{cases} \quad (4)$$

189 **Step 5:** Calculate GTDI:

$$V_{gtdi} = \alpha_{spei}^* V_{spei}^T + \alpha_{ssmi}^* V_{ssmi}^T \quad (5)$$

190 Where V_{gtdi} is the combined vector of GTDI, α_{spei}^* and α_{ssmi}^* are the normalized weight coefficients of
 191 SPEI and SSMI, respectively.

192 3.3 Classification criteria for drought

193 **Table 2.** Drought classification criteria for the SPEI, SSMI, GTDI and ETDI.

Grade	Classification	Values
1	No drought	-0.5 < Index
2	Mild drought	-1.0 < Index ≤ -0.5
3	Moderate drought	-1.5 < Index ≤ -1.5
4	Severe drought	-2.0 < Index ≤ -1.5
5	Extreme drought	Index ≤ -2.0

194 The calculating approach of SSMI in this study is comparable to that of SPEI, while GTDI and
 195 ETDI are built on SSMI and SPEI. As a result, as indicated in Table 2, the SSMI, GTDI, and ETDI



196 use the same grading criteria as the SPEI.

197 **3.4 Reliability verification**

198 **3.4.1 Evaluation of correlation**

199 A correlation analysis of the integrated drought index with two single-type drought indices is
200 necessary to assess the consistency of indicators before and after coupling. Thus, the Pearson's
201 correlation coefficients (PCC) between GTDI/ETDI with SPEI and SSMI are calculated for each
202 grid (Eq. 6), and their correlation in different locations is explored. Table 3 shows the correlation
203 levels and corresponding absolute value range of PCC.

$$PCC_{x,y} = \frac{\sum_{i=1}^n (x_i - \bar{x})(y_i - \bar{y})}{\sqrt{\sum_{i=1}^n (x_i - \bar{x})^2 \sum_{i=1}^n (y_i - \bar{y})^2}} \quad (6)$$

204 Where n denotes the sample size; x_i and y_i are data samples of x and y , respectively; \bar{x} and \bar{y} are
205 arithmetic average of x and y , respectively.

206 **Table 3.** The absolute value range of PCC and correlation levels.

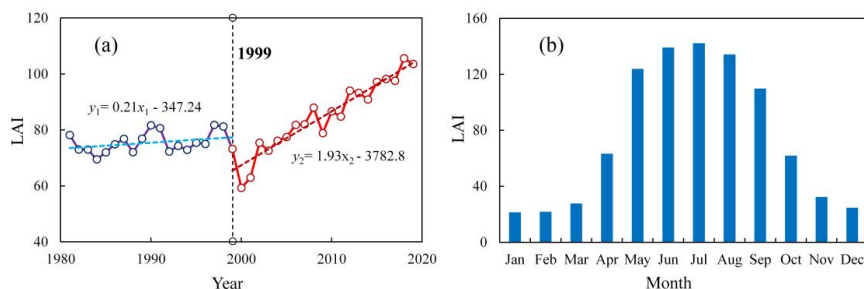
Correlation levels	Absolute values of PCC
Greatly low or none	[0, 0.2]
Low	(0.2, 0.4]
Moderate	(0.4, 0.6]
High	(0.6, 0.8]
Greatly high	(0.8, 1.0]

207 **3.4.2 Efficacy verification in identifying drought**

208 Because surface vegetation is highly sensitive to soil moisture (Li et al., 2022), drought usually leads
209 to a decrease in vegetation Leaf Area Index (LAI; Fang et al., 2019; Bock et al., 2023). In light of
210 this, LAI data are used to evaluate the drought recognition capabilities of various indexes to further
211 validate their dependability. The leaf area index dataset used is the GLOBMAP leaf area index



212 product (<https://www.resdc.cn/>).



213

214 **Figure 2.** The plot graphs of the Leaf Area Index (LAI) in the Wei River Basin with an interannual

215 trend spanning from 1981 to 2019 (a) and the average monthly allocation from 1981 to 1999 (b).

216 Significant disparities in LAI trends can be identified in the WRB around 1999, as illustrated
217 in Fig. 2(a). Prior to 1999, the average annual growth rate of LAI was only 0.21/a, but it skyrocketed
218 to 1.93/a after 1999, owing mostly to "Grain for Green" (Li et al., 2019; Tian et al., 2022). In order
219 to mitigate the potential inaccuracy resulting from the regional LAI trend change, we selected the
220 validation years of 1981 to 1999, during which the growth trend was relatively weak. Also, LAI in
221 the WRB rises significantly from March to August, falls fast from September to November, and then
222 remains low from December to January of the following year (Fig. 2b). It can be discovered that
223 LAI's trend change in autumn and winter is the result of vegetation's natural growth cycle, resulting
224 in a reduced sensitivity of LAI to soil moisture and further failing to identify drought. As a result,
225 the autumn and winter months (September to January) should also be excluded from the validation
226 period.

227 In summary, LAI raster data from March to August (spring and summer) of the period from
228 1981 to 1999 were selected to verify the drought identification efficacy of drought indices.
229 Meanwhile, the image from the mid-month of each month is regarded as the representative data of



230 the month. If the occurrence of drought has been discovered, it can be determined by comparing the
231 mean drought index values during arid months with non-arid months. The specific process is as
232 follows:

$$\begin{cases} M_{d,i} = \frac{\sum_{j=1}^m I_{i,j}}{m} \\ M_{n,i} = \frac{\sum_{l=1}^n I_{i,l}}{n} \end{cases} \quad (7)$$

$$R_i = \begin{cases} 1, M_{d,i} < M_{n,i} \\ 0, M_{d,i} \geq M_{n,i} \end{cases} \quad (8)$$

233 Where $M_{d,i}$ and $M_{n,i}$ represent the average values of the drought index in the i -th grid during arid
234 and non-arid months, respectively; m and n are the number of arid and non-arid months, respectively;
235 $I_{i,j}$ and $I_{i,l}$ represent the drought index value of the i -th grid during the j -th arid month and the l -th
236 non-arid month, respectively; R_i represents the drought recognition performance of the drought
237 index in the i -th grid, with a value of 1 indicating fine and 0 indicating poor.

238 **3.5 Analysis methods for drought characteristics**

239 **3.5.1 Mann-Kendall test**

240 The Mann-Kendall (M-K) test is a non-parametric statistical test method with a simple
241 computational process. It has been extensively utilized for the analysis of hydrological and
242 meteorological sequences (Zhang et al., 2021; Agbo et al., 2023). In this study, the M-K test method
243 is used to perform trend testing on the drought index sequences, and the calculation principle can
244 be referred to Cai et al. (2022).

245 **3.5.2 Drought identification**

246 Drought is often identified by two factors: the drought index threshold and the drought area



247 threshold. In this study, we used -1 as the drought index threshold, which is compatible with current
 248 research (Deng et al., 2021; Feng et al., 2023), and 1.6% as the area threshold (Wang et al., 2011).
 249 Furthermore, a spatiotemporal continuity technique is used to detect drought occurrences, with
 250 specific procedures available in Deng et al. (2021).

251 3.5.3 Spatiotemporal characteristics of drought

252 The spatiotemporal characteristics of drought mostly manifest in variables such as drought intensity,
 253 drought area, drought duration, and drought centroid (Wen et al., 2020). Based on the current
 254 research methods for studying the spatiotemporal characteristics of drought, we divided the
 255 variables representing drought characteristics into two scales: grid point and monthly, in order to
 256 systematically analyze and describe the drought characteristics of the WRB.

257 (1) Grid point's drought characteristic variable

258 The drought intensity S_i of the grid point is calculated by:

$$S_i = S_0 - I_i \quad (9)$$

259 Where I_i is the value of the i -th drought grid point; S_0 is the threshold of the drought index.

260 (2) Monthly drought characteristic variables

261 The monthly drought characteristic variables consist of the monthly drought intensity S_{am} , the
 262 monthly drought area A_{am} , and the monthly drought centroid (X_{am}, Y_{am}) , as shown in Table 4.

263 **Table 4.** Monthly drought characteristic variables.

Variables	Formula	Notes	Number
Monthly drought intensity S_{am}	$S_{am} = \frac{1}{k} \sum_{i=1}^k S_i$	Where k is the number of drought grids; S_i is the intensity value of the i -th drought grid.	(10)
Monthly drought area $A_{am}/10^4\text{km}^2$	$A_{am} = kA$	Where A is the spatial range of a single grid, and its unit is 10^4km^2 .	(11)



$$\text{Monthly drought centroid } (X_{am}, Y_{am}) \begin{cases} X_{am} = \sum_{i=1}^k S_i x_i / \sum_{i=1}^k S_i \\ Y_{am} = \sum_{i=1}^k S_i y_i / \sum_{i=1}^k S_i \end{cases} \quad (12)$$

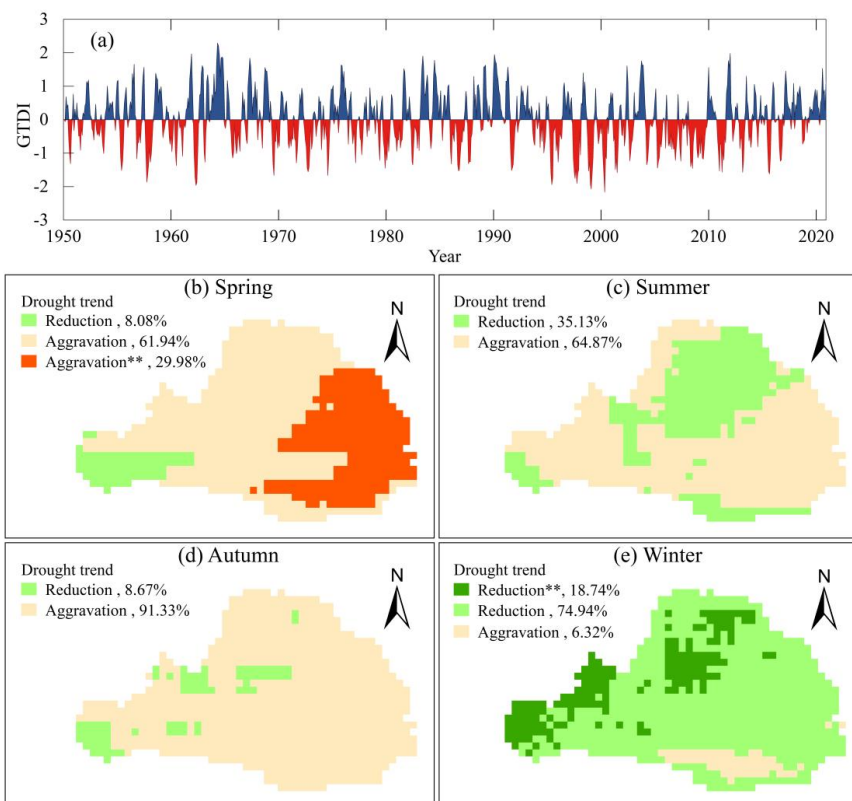
Where S_i is the drought intensity value of the i -th drought grid, and x_i and y_i are the longitude and latitude coordinates of the i -th drought grid, respectively.

264 4 Results and Discussion

265 4.1 Evolutionary characteristics of integrated drought index GTDI

266 Using the game theory method, the monthly GTDI of the WRB was calculated based on SPEI and
267 SSMI. Meanwhile, considering the WRB's seasonal characteristics, GTDI sequences from May,
268 August, November, and February of the next year were chosen to represent the drought conditions
269 of spring, summer, autumn, and winter, respectively.

270 Fig. 3(a) demonstrates the temporal evolution characteristics of the monthly GTDI in the WRB
271 from 1950 to 2020. Therein, the linear tendency rate of GTDI is $-0.024/10a$, illustrating that the
272 drought in the WRB is aggravating, which is also mentioned in Wang et al. (2020). Particularly since
273 the 1990s, the frequency of moderate and severe drought months and their average drought intensity
274 have increased by 5.1% (from 34.1% to 39.2%) and 0.043 (from 0.242 to 0.285), respectively. In
275 terms of seasonal change, drought in the WRB showed an increasing trend in spring, summer, and
276 autumn (Fig. 3b-d). In the eastern half of the WRB, the significantly aggravated area of spring
277 drought accounts for 29.98% of the overall basin, while most places in summer and autumn show a
278 non-significant aggravation in drought severity. Winter is an exception, as most areas experience a
279 reduction in drought, especially in the eastern and northern regions of the WRB (Fig. 3e).



280

281 **Figure 3.** Temporal evolution characteristics of integrated drought in the Wei River Basin from 1950

282 to 2020 (a), and spatial distribution of drought trends in different seasons (b-e). The symbol “**”

283 donates the change is significant, and the percentage means the area proportion of different trend

284 types.

285 4.2 Reliability verification of the GTDI

286 4.2.1 The evaluation of correlation

287 Table 5 illustrates the grid proportions of different correlation levels between the integrated drought

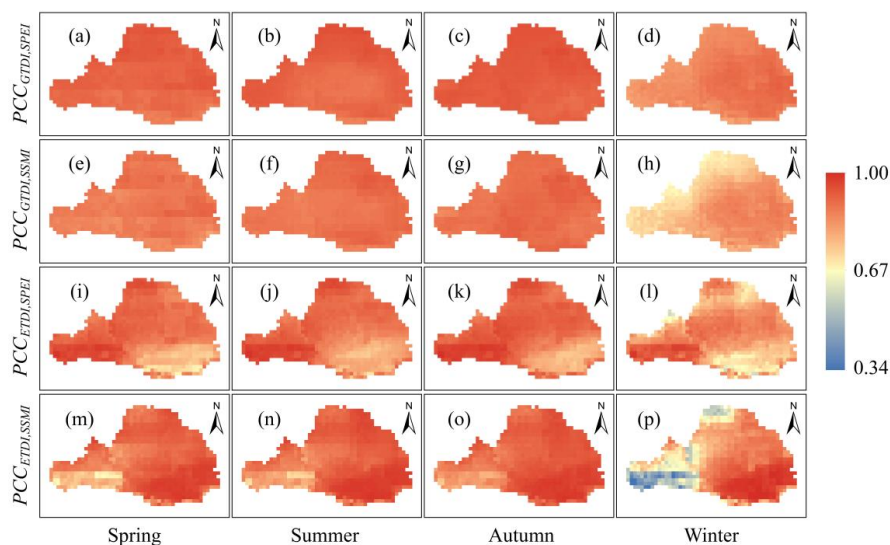
288 indices (GTDI and ETDI) and the single-type drought indices (SPEI and SSMI), whereas Fig. 5

289 depicts the spatial distribution of their correlation coefficients in different seasons.



290 **Table 5.** Grid proportions of integrated drought indices (GTDI, ETDI) and single-type drought
 291 indices (SPEI, SSMI) at different correlation levels.

Correlation levels	GTDI vs. SPEI				GTDI vs. SSMI			
	Spring	Summer	Autumn	Winter	Spring	Summer	Autumn	Winter
Greatly high	100%	100%	100%	100%	100%	100%	100%	54.8%
High	0	0	0	0	0	0	0	45.2%
Correlation levels	ETDI vs. SPEI				ETDI vs. SSMI			
	Spring	Summer	Autumn	Winter	Spring	Summer	Autumn	Winter
Greatly high	83.6%	89.5%	88.4%	66.2%	89.7%	95.6%	98.2%	68.3%
High	16.4%	10.5%	11.6%	33.3%	10.3%	4.4%	1.8%	25.8%
Moderate	0	0	0	0.5%	0	0	0	5.4%
Low	0	0	0	0	0	0	0	0.5%



292 Spring Summer Autumn Winter
 293 **Figure 4.** Spatial distribution of correlation coefficients in different seasons. The color bar on the
 294 right denotes the correlation coefficients.

295 As shown in Table 5 and Fig. 4, the correlation between GTDI and SPEI or SSMI in the entire
 296 WRB is quite significant, and the correlation coefficients (PCC) are close to 1 in spring, summer,
 297 and autumn, but slightly worse in winter (Fig. 4a-h). The correlation coefficients in the western and
 298 northern areas of the WRB are lower in winter (Fig. 4d, h, l, p), but the minimal correlation



299 coefficients between GTDI and SPEI or SSMI are still above 0.83 and 0.67, respectively (Fig. 4d,
300 h). It is worth noting that GTDI and SPEI have a greatly high correlation across the WRB over all
301 four seasons, whereas 45.2% of locations only have a good correlation between GTDI and SSMI in
302 winter (Table 5). As a result, the correlation between GTDI and SPEI is stronger than that of SSMI,
303 especially during the winter season.

304 The graph also shows that the integrated drought index (ETDI) demonstrates spatially opposite
305 correlations with SPEI and SSMI. For instance, in the southeastern area of the Wei River Basin,
306 there is the worst association between ETDI and SPEI, but the correlation between ETDI and SSMI
307 is the strongest (Fig. 4i-p). Similar to GTDI, the correlation between ETDI and SPEI or SSMI is
308 slightly higher in spring, summer, and autumn than in winter. However, as compared to GTDI, the
309 geographical variability of the correlation coefficients between ETDI and SPEI or SSMI is more
310 pronounced in the same season (Fig. 4). As seen in winter (Fig. 4p), the highest correlation
311 coefficient between ETDI and SSMI is approximately 1, while the lowest value is around 0.34. In
312 terms of grid proportions at various levels of correlation, the correlations between ETDI and SPEI
313 or SSMI do not achieve a greatly high level in certain regions over the four seasons (Table 5),
314 resulting in their performance falling short compared to GTDI.

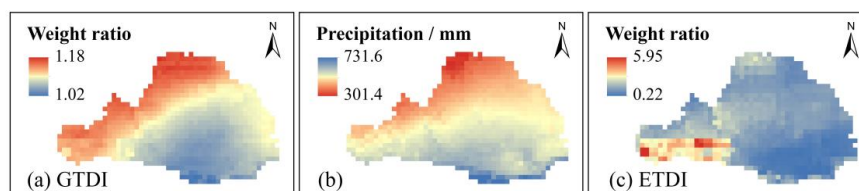
315 Overall, GTDI exhibits superior performance to ETDI, particularly in terms of the homogeneity
316 of the spatial distribution of correlation coefficients, indicating that the integrated drought index
317 GTDI constructed in this study has more reliable consistency with single-type drought indices (SPEI
318 and SSMI).

319 **4.2.2 Comparison of the integrated weight of GTDI and ETDI**

320 To contrast the weight distribution of SPEI and SSMI in creating the integrated drought indices



321 GTDI and ETDI, the spatial distribution of their weight ratios (SPEI/SSMI) in the WRB is plotted,
322 as shown in Fig. 5.



323
324 **Figure 5.** Comparison of the integrated weights of GTDI and ETDI. Subfigures (a) and (c)
325 demonstrate the spatial distribution of weight ratio (SPEI/SSMI) in the construction process of
326 GTDI and ETDI, respectively, and (b) is a spatial distribution map of the average annual
327 precipitation in the Wei River Basin.

328 The GTDI, a comprehensive drought index constructed using the game theory method, exhibits
329 a spatial distribution of the weight ratio (SPEI/SSMI) that gradually decreases from northwest to
330 southeast (Fig. 5a). Furthermore, the weight ratio in GTDI ranges from 1.02 to 1.18, showing a
331 substantially balanced weight allocation between the hazard-causing index (SPEI) and the hazard-
332 bearing index (SSMI). Meanwhile, the weight ratio of SPEI to SSMI is closer to 1 in places with
333 greater precipitation (Fig. 5a-b). It is noteworthy that the change in weight ratio (SPEI/SSMI) in
334 GTDI closely resembles the spatial distribution pattern of the average annual precipitation in the
335 WRB, as evidenced by a correlation coefficient of -0.88, indicating a significant negative
336 relationship.

337 The entropy theory-based drought index (ETDI), on the other hand, does not show a distinct
338 spatial distribution pattern for the weight ratio of SPEI to SSMI. Its weight ratio fluctuates greatly
339 between locations, ranging from 0.22 to 5.95 (Fig. 5c), implying that entropy theory fails to establish
340 a consistently stable allocation of weights in the integrated drought index ETDI development



341 process. Furthermore, the weight ratio (SPEI/SSMI) in ETDI has a low relationship with annual
342 average precipitation, as evidenced by a correlation coefficient of only -0.04.

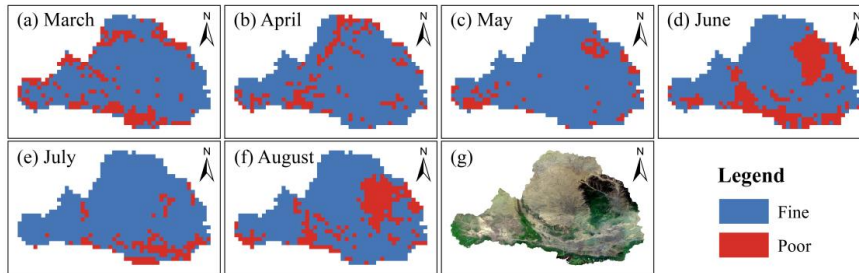
343 As a consequence of comparing GTDI and ETDI, it is discovered that the game theory
344 approach gives an integrated weight geographic distribution compatible with the precipitation-
345 dominated natural drought pattern, which is essentially congruent with the drought generation
346 mechanism in this basin. As a result, it is thought that the weighting of SPEI and SSMI in GTDI is
347 more reasonable and reliable.

348 **4.2.3 The efficacy verification in identifying drought**

349 To further investigate the reliability of the integrated drought index GTDI, the Leaf Area Index (LAI)
350 data is used to assess its efficacy in identifying drought, and the drought recognition performance
351 of the GTDI is evaluated by Eq. 8 and presented in Fig. 6. To compare, Fig. 7 depicts the spatial
352 distribution of efficacy in recognizing drought using the ETDI, SPEI, and SSMI, and Table 6
353 provides a statistical list exhibiting the efficacy ratios of four drought indices in different validation
354 months.

355 **Table 6.** The efficacy ratios of four drought indices in different validation months

Drought indices	March	April	May	June	July	August
GTDI	78.6%	84.1%	90.4%	71.8%	87.5%	76.3%
ETDI	48.4%	49.6%	50.7%	50.5%	49.2%	48.6%
SPEI	50.1%	49.5%	50.6%	49.4%	48.4%	48.8%
SSMI	49.1%	50.4%	52.8%	49.9%	49.5%	48.9%

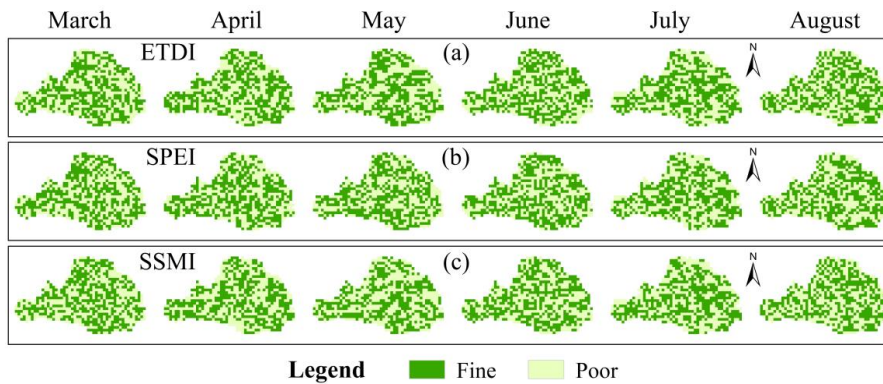


356

357 **Figure 6.** The spatial distribution of GTDI's efficacy in identifying drought in the Wei River Basin.

358 Subfigures (a)-(f) depict the findings from March to August, and (g) displays a satellite image of the

359 Wei River Basin.



360

361 **Figure 7.** The spatial distribution of efficacy in identifying drought of the ETDI, SPEI and SSMI.

362 During the validation period from March to August, GTDI performs well in recognizing
 363 drought (Fig. 6), particularly in May, when it captures 90.28% of the drought in the WRB (Table 6).

364 GTDI, on the other hand, performs relatively badly in June (Fig. 6d) and August (Fig. 6f), only with
 365 71.8% and 76.3% of effective recognition grid points, respectively (Table 6). In conjunction with

366 Fig. 6(g), it is discovered that the grid points with poor performance in June and August are
 367 concentrated in the forest area, which is the dark green area in the WRB's northeast hinterland. As

368 is widely known, forests have more access to deeper soil moisture than farming land and grassland
 369 (Xu et al., 2018; Bai et al., 2023), resulting in forests having higher drought tolerance than other



370 terrestrial vegetation types (Jiang et al., 2020; Chen et al., 2022). However, the soil moisture data
371 used in this study is only 0 to 10cm of soil surface layer, which could explain why GTDI's drought
372 diagnosis ability in the forest region is skewed. Even with the defect in forest regions, GTDI has
373 exhibited strong drought monitoring capabilities in the WRB, and can effectively capture the
374 occurrence of drought.

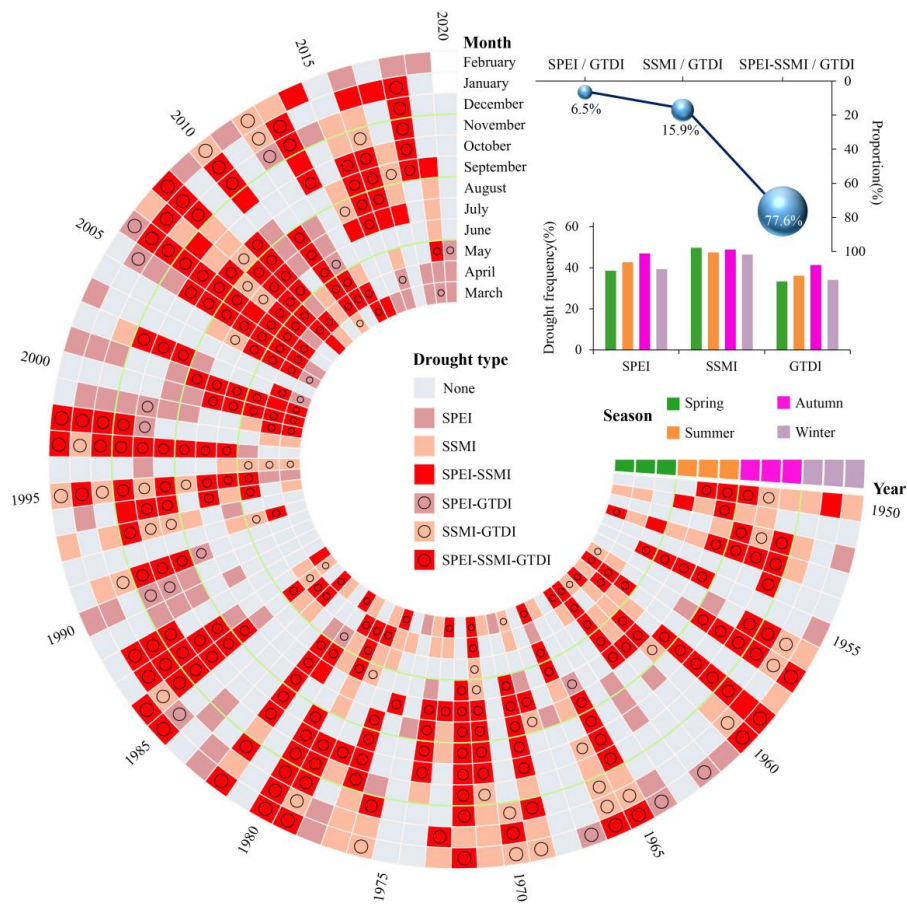
375 In contrast to GTDI, the effectiveness of drought detection by ETDI, SPEI, and SSMI is
376 geographically random and chaotic, as illustrated in Fig. 7. Furthermore, in all validation months,
377 ETDI, SPEI, and SSMI only provide efficacy ratios of around 50%, indicating a lack of significant
378 usefulness in identifying drought (Table 6). As a result, when compared to ETDI, SPEI, and SSMI,
379 it is clear that GTDI provides significant advantages in the field of drought monitoring. To
380 summarize, GTDI does not simply combine the hazard-causing index (SPEI) and the hazard-bearing
381 index (SSMI) as ETDI, but it can indeed capture drought occurrence in most areas, addressing the
382 issue of single-type drought indices' insufficient responsiveness to actual drought events.

383 **4.3 Comparison of temporal trajectories of drought identified by** 384 **GTDI, SPEI, and SSMI**

385 The drought identification trajectories of the integrated drought index (GTDI), single-type drought
386 indices (SPEI and SSMI) during the study period are depicted in Fig. 8. Out of the 850 months
387 spanning from March 1950 to December 2020, merely 345 months are devoid of any drought,
388 accounting for approximately 40.6% of the total, which contradicts our common understanding of
389 drought incidents. Among the 505 dry months, 409 months experience agricultural drought (SSMI,
390 48.1%), 356 months experience meteorological drought (SPEI, 41.9%), and 260 months (30.6%)



391 experience both simultaneously. GTDI identifies just 308 arid months (36.2%) out of 850 months,
 392 which is lower than SSMI and SPEI. According to the data presented above, agricultural drought
 393 has been the most common occurrence in the WRB over the last 70 years, followed by
 394 meteorological drought, with GTDI identifying the fewest number of drought months.



395
 396 **Figure 8.** Comparison of the SPEI, SSMI and GTDI in temporal drought trajectories. "SPEI-SSMI"
 397 means that it is recognized as a drought month by SPEI and SSMI simultaneously, and the meanings
 398 of other drought types are similar to that.

399 Out of the GTDI-identified drought months, the proportion of meteorological drought
 400 occurring alone is 6.5%, and the proportion of agricultural drought occurring alone is 15.9%,



401 possibly due to high temperatures, while the proportion of meteorological drought and agricultural
402 drought occurring simultaneously is up to 77.6%. Thus, it is clear that GTDI is closely related to the
403 hazard-causing index (SPEI) and the hazard-bearing index (SSMI) and is caused by both in most
404 cases. It corresponds to the general public's understanding of drought incidents. Furthermore,
405 because it is calculated by weighting SPEI and SSMI, GTDI has an advantage in depicting the
406 temporal gaming evolution of SPEI and SSMI. From the perspective of seasonal distribution,
407 meteorological drought occurs most commonly in the summer and autumn, with a frequency of
408 more than 40%, but less frequently in the winter and spring. At the same time, agricultural drought
409 (SSMI) occurs at a frequency of over 45% in all seasons, with a very similar frequency in four
410 seasons. The seasonal allocation mode of drought identified by GTDI is similar to that of SPEI, with
411 the similarity being that it occurs more frequently in summer and autumn than in winter and spring.
412 However, the frequency of drought determined by SPEI is slightly higher than that determined by
413 GTDI in each season.

414 The above explanation suggests that using SPEI, SSMI, and GTDI for monthly-scale drought
415 identification may result in various drought trajectories. Meanwhile, the GTDI is a hybrid of the
416 hazard-causing index (SPEI) and the hazard-bearing index (SSMI), as it has a higher overlap with
417 SSMI in drought trajectory, implying changes in the hazard-bearing body during the dry period,
418 while being closer to SPEI in drought seasonal allocation, responding to the fluctuation of hazard-
419 causing factors. When paired with the GTDI index reliability analysis in Section 4.2, it is concluded
420 that the occurrence of drought events in the Wei River Basin is still dominated by precipitation
421 deficiency, and the region is located in a dry location with low rainfall.

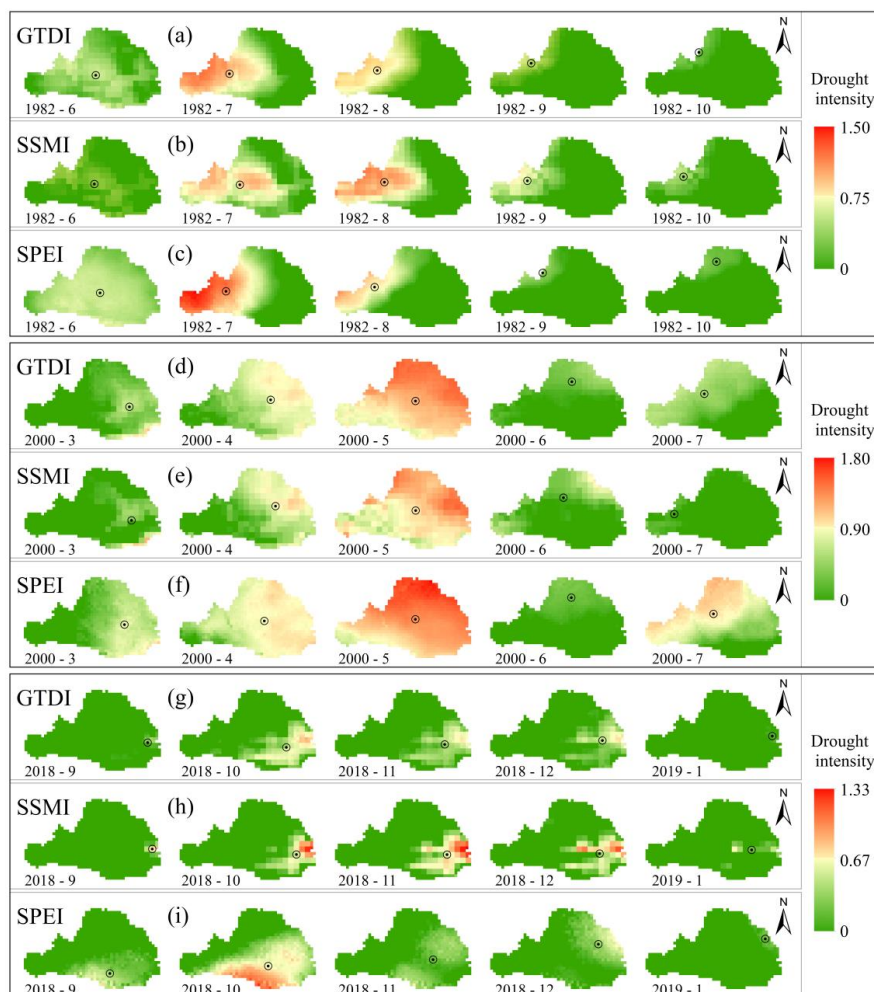


422 **4.4 Comparison of spatial evolution of drought events identified by**
 423 **GTDI, SPEI, and SSMI**

424 To explore the spatial development process of drought occurrences recognized by GTDI, SPEI, and
 425 SSMI while eliminating the randomness of a single event, we selected three drought events that
 426 lasted for a duration of 5 months for spatial evolution analysis. Fig. 9 shows the spatial evolution
 427 processes of three drought events identified by GTDI, SPEI, and SSMI, spanning from June to
 428 October 1982, from March to July 2000, and from September 2018 to January 2019, respectively.
 429 Table 7 shows the drought intensity and the percentage of drought area for each month of the three
 430 drought events.

431 **Table 7.** Comparison of SPEI, SSMI and GTDI in drought intensity and percentage of drought area
 432 during three drought events

Drought events	Year-month	Drought intensity			Percentage of drought area		
		SPEI	GTDI	SSMI	SPEI	GTDI	SSMI
1982	1982-6	0.47	0.31	0.28	100%	85.9%	55.7%
	1982-7	0.77	0.66	0.55	63.2%	67.0%	81.5%
	1982-8	0.52	0.57	0.71	42.5%	49.3%	58.5%
	1982-9	0.17	0.22	0.37	15.0%	23.3%	35.9%
	1982-10	0.15	0.13	0.22	17.4%	14.1%	22.4%
2000	2000-3	0.49	0.32	0.29	74.1%	61.2%	32.3%
	2000-4	0.82	0.66	0.58	98.2%	92.7%	79.3%
	2000-5	1.29	1.17	1.03	100%	100%	100%
	2000-6	0.18	0.21	0.31	38.4%	50.1%	54.3%
2018	2018-7	0.76	0.41	0.11	87.0%	66.6%	15.5%
	2018-9	0.23	0.10	0.33	35.9%	5.3%	3.0%
	2018-10	0.55	0.41	0.46	65.6%	34.2%	21.0%
	2018-11	0.20	0.31	0.55	46.5%	32.4%	28.7%
	2018-12	0.22	0.27	0.46	43.3%	31.0%	27.5%
	2019-1	0.11	0.06	0.22	5.3%	1.8%	7.5%



433

434 **Figure 9.** Comparison of SPEI, SSMI and GTDI in the spatial evolution of three drought events.

435 The black circle donates the monthly drought centroid.

436 Taking the 1982 drought event as an example, the meteorological drought emerges initially,
437 followed by a steady decrease in its impact areas (Fig. 9c). However, the overall drought intensity
438 increases and subsequently decreases (Table 7), and the drought centroid migrates from the WRB's
439 center to the northwest. It is worth noting that concurrent agricultural drought lags behind
440 meteorological drought. When comparing the drought geographic evolution processes identified by



441 SSMI and SPEI (Fig. 9b-c), the lag period is approximately one month, which is similarly observed
442 in the other two drought events (Fig. 9d-i). For the entire spatial evolution process of a drought event
443 identified by GTDI, it is clear that its spatial pattern is the result of a compromise of SPEI and SSMI,
444 including the migration path of the drought centroid (Fig. 9a-c), the evolution process of drought
445 area percentage, and drought intensity (Table 7).

446 From March to July 2000, the WRB experienced a fully covered drought event (Fig. 9d-f),
447 which began with a meteorological drought. The fusion description of SPEI and SSMI produced by
448 GTDI during this event, which incorporates the spatial evolution trends of SPEI and SSMI to
449 evaluate the current drought status at each grid point, may be observed. The value of GTDI
450 consistently falls between SPEI and SSMI, regardless of whether it is evaluated by the drought area
451 ratio, drought intensity, or drought centroid.

452 The 2018 drought event is the mildest of the three, but it most fully depicts the process of a
453 drought event from emergence to spread to eventual extinction (Fig. 9g-i). In the early stages of this
454 drought event, as of October 2018, the meteorological drought in the southeastern part of the WRB
455 was the most severe, whilst the agricultural drought was relatively negligible. In this case, the spatial
456 drought pattern determined by GTDI was closer to the development of hazard-causing index SPEI.
457 However, during the later stages of the drought event, the situation reverses and the spatial evolution
458 of drought begins to be dominated by the hazard-bearing index SSMI, illustrating GTDI possesses
459 more realistic and intelligent feature in drought identification. This also demonstrates the
460 importance of including game theory in this study, which has a distinct benefit in monitoring
461 changes in hazard-causing and bearing impacts.

462 Based on the foregoing, it is worth noting that the GTDI-identified spatial drought process



463 combines the evolutionary features of hazard-causing and bearing indices (SPEI and SSMI). In
464 addition, merging SPEI and SSMI via their game relationship, rather than simply putting them
465 together, makes GTDI a superior technique to represent the spatial and temporal evolution of
466 droughts. Furthermore, it has been discovered that the GTDI exhibits the gaming feature of the
467 drought hazard-causing and bearing index. This is evidenced by the fact that the hazard-causing
468 index SPEI primarily drives the early stages of drought events in the WRB, while the hazard-bearing
469 index SSMI primarily drives the later stages.

470 **5 Conclusions**

471 This study integrated the SPEI (meteorological index and drought hazard-causing index) and SSMI
472 (agricultural index and drought hazard-bearing index) to propose a game theory-based drought index
473 (GTDI). The integration performance and weight allocation of the GTDI were demonstrated by
474 evaluating the correlations with SPEI and SSMI, and comparing the integrated weight to the ETDI
475 (entropy theory-based drought index); the reliability of the GTDI was confirmed by the Leaf Area
476 Index (LAI) data; and the advancedness of the GTDI was examined by contrasting the temporal
477 trajectories and spatial evolution characteristics of GTDI, SPEI, and SSMI. The following are the
478 primary conclusions:

479 The single-type drought indices (SPEI and SSMI) and the integrated drought index (GTDI)
480 exhibit dependable spatial consistency. In all locations within the Wei River Basin during the four
481 seasons, there is a greatly high correlation between GTDI and SPEI. The correlation between GTDI
482 and SSMI is relatively weak in the winter, only reaching a high correlation in 54.8% of the basin,
483 while it continues to have exceptionally high correlations throughout the basin during the other three



484 seasons.

485 The entropy theory-based drought index ETDI performs worse than the GTDI, particularly
486 when it comes to the regional distribution of correlation coefficient homogeneity. Specially, the
487 game theory technique provides an integrated weight geographic distribution in the integrated index
488 GTDI that is consistent with the precipitation-dominated natural drought pattern. Furthermore, there
489 is a strong negative spatial relationship between the weight ratio of SPEI to SSMI and the average
490 annual precipitation in the Wei River Basin, with a correlation coefficient of -0.88. The ETDI, on
491 the other hand, has a very weak connection (correlation coefficient of -0.04) with the annual mean
492 precipitation. This indicates that the GTDI's weight distribution of SPEI and SSMI is more logical
493 and trustworthy.

494 The GTDI has superior efficacy for identifying drought when compared to the ETDI, SPEI,
495 and SSMI. When drought occurs, GTDI efficiently captures it with an efficacy ratio of over 70% in
496 all validation months, whereas ETDI, SPEI, and SSMI catch it with an efficacy ratio of
497 approximately 50%. In terms of drought impact, GTDI can capture drought occurrence in most
498 places but fails in the forest due to insufficient depth of soil surface layer measurement, whereas
499 ETDI, SPEI, and SSMI drought detection are geographically random and chaotic. Thus, GTDI is
500 expected to replace single-type drought indices to provide a more accurate portrayal of actual
501 drought.

502 The GTDI merges SPEI and SSMI via their game relationship rather than simply putting them
503 together, making it a superior technique to represent the spatial and temporal evolution of droughts.
504 Due to the GTDI is a hybrid of the hazard-causing index (SPEI) and the hazard-bearing index
505 (SSMI), it represents diverse drought trajectories identified by the monthly-scale SPEI and SSMI.



506 Specially, it has a higher overlap with SSMI in drought trajectory, implying changes in the hazard-
507 bearing body during the dry period, while being closer to SPEI in drought seasonal allocation,
508 responding to the fluctuation of hazard-causing factors. Additionally, it has been discovered that
509 GTDI exhibits the gaming feature of the drought hazard-causing and bearing index, having a distinct
510 benefit in monitoring changes in their impacts.

511 According to an investigation of monthly GTDI in the Wei River Basin from 1950 to 2020,
512 there is a growing propensity for drought, particularly since the 1990s, when the intensity and
513 frequency of drought in the WRB have increased significantly. Drought deterioration is most visible
514 in the spring, insignificant in the summer and autumn, and most areas embrace drought reduction in
515 the winter. Drought events in the Wei River Basin are dominated by a lack of precipitation. The
516 hazard-causing index SPEI dominates the early stages of a drought event, whereas the hazard-
517 bearing index SSMI dominates the later stages.

518 **Data availability**

519 All produced data can be provided by the corresponding author upon request.

520 **Author contribution**

521 Conceptualization: HZ; data curation: YZ; formal analysis: ZY; methodology: TL; investigation:
522 XZ; software: ZY; visualization: TL; writing – original draft: XZ; writing – review and editing: TY;
523 supervision: HZ; funding acquisition: HZ; project administration: HZ; validation: CX; resources:
524 HZ. All authors have read and agreed to publish the manuscript.

525 **Competing interests**

526 The authors declare that they have no conflict of interest.



527 **Acknowledgments**

528 This research is supported by the National Natural Science Foundation of China (51979005), the
529 Natural Science Basic Research Program of Shaanxi Province (2022JC-LHJJ-03) and the
530 Fundamental Research Funds for the Central Universities (300102293201). Our cordial thanks
531 should be extended to the editor and anonymous reviewers for their pertinent and professional
532 suggestions and comments which are greatly helpful for further improvement of the quality of this
533 paper.

534

535 **Reference**

- 536 Agbo, E.P., Nkajoe, U., and Edet, C.O.: Comparison of Mann–Kendall and Şen’s innovative trend
537 method for climatic parameters over Nigeria’s climatic zones, *Clim Dyn.*, 60, 3385-3401,
538 <https://doi.org/10.1007/s00382-022-06521-9>, 2023.
- 539 AghaKouchak, A., Huning, L.S., Sadegh, M., Qin, Y., Markonis, Y., Vahedifard, F., Love, C.A.,
540 Mishra, A., Mehran, A., Obringer, R., Hjelmstad, A., Pallickara, S., Jiwa, S., Hanel, M., Zhao, Y.,
541 Pendergrass, A.G., Arabi, M., Davis, S.J., Ward, P.J., Svoboda, M., Pulwarty, R., and Kreibich,
542 H.: Toward impact-based monitoring of drought and its cascading hazards, *Nat. Rev. Earth*
543 *Environ.*, 4, 582-595, <https://doi.org/10.1038/s43017-023-00457-2>, 2023.
- 544 Bai, Y., Liu, M., Guo, Q., Wu, G., Wang, W., and Li, S.: Diverse responses of gross primary
545 production and leaf area index to drought on the Mongolian Plateau, *Sci. Total Environ.*, 902,
546 166507, <https://doi.org/10.1016/j.scitotenv.2023.166507>, 2023.
- 547 Batabyal, A.A. and Beladi, H.: A game-theoretic model of water theft during a drought, *Agric. Water*



- 548 Manage., 255, 107044, <https://doi.org/10.1016/j.agwat.2021.107044>, 2021.
- 549 Berg, A. and Sheffield, J.: Climate change and drought: the soil moisture perspective, *Curr. Clim.*
- 550 *Chang. Rep.*, 4, 180-191, <https://doi.org/10.1007/s40641-018-0095-0>, 2018.
- 551 Bock, A.D., Belmans, B., Vanlanduit, S., Blom, J., Alvarado-Alvarado, A.A., and Audenaert, A.: A
- 552 review on the leaf area index (LAI) in vertical greening systems, *Build. Environ.*, 229, 109926,
- 553 <https://doi.org/10.1016/j.buildenv.2022.109926>, 2023.
- 554 Cai, Y., Zhang, F., Duan, P., Jim, C.Y., Chan, N.W., Shi, J., Liu, C., Wang, J., Bahtebay, J., and Ma,
- 555 X.: Vegetation cover changes in China induced by ecological restoration-protection projects and
- 556 land-use changes from 2000 to 2020, *Catena.*, 217, 106530,
- 557 <https://doi.org/10.1016/j.catena.2022.106530>, 2022.
- 558 Chang, J., Li, Y., Wang, Y., and Yuan, M.: Copula-based drought risk assessment combined with an
- 559 integrated index in the Wei River Basin, China, *J. Hydrol.*, 540, 824-834,
- 560 <https://doi.org/10.1016/j.jhydrol.2016.06.064>, 2016.
- 561 Chen, Q., Timmermans, J., Wen, W., and van Bodegom, P.M.: A multi-metric assessment of drought
- 562 vulnerability across different vegetation types using high resolution remote sensing, *Sci. Total*
- 563 *Environ.*, 832, 154970, <https://doi.org/10.1016/j.scitotenv.2022.154970>, 2022.
- 564 Dai, A.: Drought under global warming: a review, *Wiley Interdiscipl. Rev. Clim. Change.*, 2, 45-65,
- 565 <https://doi.org/10.1002/wcc.81>, 2011.
- 566 Dai, A.: Increasing drought under global warming in observations and models, *Nat. Clim. Change.*,
- 567 3, 52-58, <https://doi.org/10.1038/nclimate1633>, 2013.
- 568 Deng, C.L., She, D.X., Zhang, L.P., Zhang, Q., Liu, X., and Wang, S.X.: Characteristics of drought
- 569 events using three-dimensional graph connectedness recognition method in the Yangtze River



- 570 Basin, China, *Trans. Chin. Soc. Agric. Eng.*, 37, 131-139, 2021.
- 571 Ding, Y., Gong, X., Xing, Z., Cai, H., Zhou, Z., Zhang, D., Sun, P., and Shi, H.: Attribution of
572 meteorological, hydrological and agricultural drought propagation in different climatic regions of
573 China, *Agric. Water Manage.*, 255, 106996, <https://doi.org/10.1016/j.agwat.2021.106996>, 2021.
- 574 Fang, H., Baret, F., Plummer, S., and Schaeppman-Strub, G.: An overview of global leaf area index
575 (LAI): Methods, products, validation, and applications, *Rev. Geophys.*, 57, 739-799,
576 <https://doi.org/10.1029/2018RG000608>, 2019.
- 577 Feng, K., Yan, Z., Li, Y., Wang, F., Zhang, Z., Su, X., Wu, H., Zhang, G., and Wang, Y.: Spatio-
578 temporal dynamic evaluation of agricultural drought based on a three-dimensional identification
579 method in Northwest China, *Agric. Water Manage.*, 284, 108325,
580 <https://doi.org/10.1016/j.agwat.2023.108325>, 2023.
- 581 Hao, Z. and AghaKouchak, A.: Multivariate standardized drought index: a parametric multi-index
582 model, *Adv. Water Resour.*, 57, 12-18, <https://doi.org/10.1016/j.advwatres.2013.03.009>, 2013.
- 583 Huang, J., Yu, H., Guan, X., Wang, G., and Guo, R.: Accelerated dryland expansion under climate
584 change, *Nat. Clim. Chang.*, 6, 166-171, <https://doi.org/10.1038/nclimate2837>, 2016.
- 585 Huang, S., Chang, J., Leng, G., and Huang, Q.: Integrated index for drought assessment based on
586 variable fuzzy set theory: a case study in the Yellow River basin, China, *J. Hydrol.*, 527, 608-618,
587 <https://doi.org/10.1016/j.jhydrol.2015.05.032>, 2015.
- 588 Jato-Espino, D. and Ruiz-Puente, C.: Bringing Facilitated Industrial Symbiosis and Game Theory
589 together to strengthen waste exchange in industrial parks, *Sci. Total Environ.*, 771, 145400,
590 <https://doi.org/10.1016/j.scitotenv.2021.145400>, 2021.
- 591 Jiang, W., Wang, L., Feng, L., Zhang, M., and Yao, R.: Drought characteristics and its impact on



- 592 changes in surface vegetation from 1981 to 2015 in the Yangtze River Basin, China, *Int. J.*
593 *Climatol.*, 40, 3380-3397, <https://doi.org/10.1002/joc.6403>, 2020.
- 594 Khorshidi, M.S., Nikoo, M.R., Sadegh, M., and Nematollahi, B.: A multi-objective risk-based game
595 theoretic approach to reservoir operation policy in potential future drought condition, *Water*
596 *Resour. Manage.*, 33, 1999-2014, <https://doi.org/10.1007/s11269-019-02223-w>, 2019.
- 597 Labudová, L., Labuda, M., and Takáč, J.: Comparison of SPI and SPEI applicability for drought
598 impact assessment on crop production in the Danubian Lowland and the East Slovakian Lowland,
599 *Theor. Appl. Climatol.*, 128, 491-506, <https://doi.org/10.1007/s00704-016-1870-2>, 2017.
- 600 Lai, C., Chen, X., Chen, X., Chen, X., Wang, Z., Wu, X., and Zhao, S.: A fuzzy comprehensive
601 evaluation model for flood risk based on the combination weight of game theory, *Nat. Hazards.*,
602 77, 1243-1259, <https://doi.org/10.1007/s11069-015-1645-6>, 2015.
- 603 Leng, G., Tang, Q., and Rayburg, S.: Climate change impacts on meteorological, agricultural and
604 hydrological droughts in China, *Glob. Planet. Chang.*, 126, 23-34,
605 <https://doi.org/10.1016/j.gloplacha.2015.01.003>, 2015.
- 606 Li, G., Sun, S., Han, J., Yan, J., Liu, W., Wei, Y., Lu, N., and Sun, Y.: Impacts of Chinese Grain for
607 Green program and climate change on vegetation in the Loess Plateau during 1982–2015, *Sci.*
608 *Total Environ.*, 660, 177-187, <https://doi.org/10.1016/j.scitotenv.2019.01.028>, 2019.
- 609 Li, L., She, D., Zheng, H., Lin, P., and Yang, Z.: Elucidating diverse drought characteristics from
610 two meteorological drought indices (SPI and SPEI) in China, *J. Hydrometeorol.*, 21, 1513-1530,
611 <https://doi.org/10.1175/JHM-D-19-0290.1>, 2020.
- 612 Li, W., Migliavacca, M., Forkel, M., Denissen, J.M.C., Reichstein, M., Yang, H., Duveiller, G.,
613 Weber, U., and Orth, R.: Widespread increasing vegetation sensitivity to soil moisture, *Nat.*



- 614 Commun., 13, 3959, <https://doi.org/10.1038/s41467-022-31667-9>, 2022.
- 615 Liu, B., Huang, J.J., McBean, E., and Li, Y.: Risk assessment of hybrid rain harvesting system and
616 other small drinking water supply systems by game theory and fuzzy logic modeling, *Sci. Total*
617 *Environ.*, 708, 134436, <https://doi.org/10.1016/j.scitotenv.2019.134436>, 2020.
- 618 Liu, Y., Zhu, Y., Ren, L., Yong, B., Singh, V.P., Yuan, F., Jiang, S., and Yang, X.: On the mechanisms
619 of two composite methods for construction of multivariate drought indices, *Sci. Total Environ.*,
620 647, 981-991, <https://doi.org/10.1016/j.scitotenv.2018.07.273>, 2019.
- 621 Ma, B., Zhang, B., Jia, L., and Huang, H.: Conditional distribution selection for SPEI-daily and its
622 revealed meteorological drought characteristics in China from 1961 to 2017, *Atmos. Res.*, 246,
623 105108, <https://doi.org/10.1016/j.atmosres.2020.105108>, 2020.
- 624 Madani, K.: Game theory and water resources, *J. Hydrol.*, 381, 225-238,
625 <https://doi.org/10.1016/j.jhydrol.2009.11.045>, 2010.
- 626 McKee, T.B., Doesken, N.J., and Kleist, J.: The relationship of drought frequency and duration to
627 time scales, Paper Presented at Proceedings of the 8th Conference on Applied Climatology, 17,
628 179-183, 2010.
- 629 Ministry of Water Resources of China: China Flood and Drought Disaster Prevention Bulletin,
630 China Water Power Press, Beijing, 2022.
- 631 Oertel, M., Meza, F.J., Gironás, J., Scott, C.A., Rojas, F., and Pineda-Pablos, N.: Drought
632 propagation in semi-arid river basins in Latin America: lessons from Mexico to the Southern Cone,
633 *Water*, 10, 1564, <https://doi.org/10.3390/w10111564>, 2018.
- 634 Palmer, W.C.: Meteorological drought, US Department of Commerce, Weather Bureau, Washington,
635 DC, 1965.



- 636 Saha, A., Pal, S.C., Chowdhuri, I., Roy, P., Chakraborty, R., and Shit, M.: Vulnerability assessment
637 of drought in India: Insights from meteorological, hydrological, agricultural and socio-economic
638 perspectives, *Gondw. Res.*, 123, 68-88, <https://doi.org/10.1016/j.gr.2022.11.006>, 2023.
- 639 Shah, D., and Mishra, V.: Integrated Drought Index (IDI) for drought monitoring and assessment in
640 India, *Water Resour. Res.*, 56, e2019WR026284, <https://doi.org/10.1029/2019WR026284>, 2020.
- 641 Shukla, S., and Wood, A.W.: Use of a standardized runoff index for characterizing hydrologic
642 drought, *Geophys. Res. Lett.*, 35, <https://doi.org/10.1029/2007GL032487>, 2008.
- 643 Tan, Y.X., Ng, J.L., and Huang, Y.F.: Quantitative analysis of input data uncertainty for SPI and
644 SPEI in Peninsular Malaysia based on the bootstrap method, *Hydrol. Sci. J.*, 68, 1724-1737,
645 <https://doi.org/10.1080/02626667.2023.2232348>, 2023.
- 646 Tian, P., Liu, L., Tian, X., Zhao, G., Klik, A., Wang, R., Lu, X., Mu, X., and Bai, Y.: Sediment yields
647 variation and response to the controlling factors in the Wei River Basin, China, *Catena.*, 213,
648 106181, <https://doi.org/10.1016/j.catena.2022.106181>, 2022.
- 649 Trenberth, K.E., Dai, A., Van, and van der Schrier, G.: Global warming and changes in drought, *Nat.*
650 *Clim. Change.*, 4, 17-22, <https://doi.org/10.1038/nclimate2067>, 2014.
- 651 Vicente-Serrano, S.M., Beguería, S., and López-Moreno, J.I.: A multiscalar drought index sensitive
652 to global warming: the standardized precipitation evapotranspiration index, *J. Clim.*, 23, 1696-
653 1718, <https://doi.org/10.1175/2009JCLI2909.1>, 2010.
- 654 Vicente-Serrano, S.M., Quiring, S.M., Pena-Gallardo, M., Yuan, S., and Domínguez-Castro, F.: A
655 review of environmental droughts: Increased risk under global warming? *Earth Sci. Rev.*, 201,
656 102953, <https://doi.org/10.1016/j.earscirev.2019.102953>, 2020.
- 657 Wang, A., Lettenmaier, D.P., and Sheffield, J.: Soil moisture drought in China, 1950–2006, *J. Clim.*,



- 658 24, 3257-3271, <https://doi.org/10.1175/2011JCLI3733.1>, 2011.
- 659 Wang, F., Wang, Z., Yang, H., Di, D., Zhao, Y., Liang, Q., and Hussain, Z.: Comprehensive
660 evaluation of hydrological drought and its relationships with meteorological drought in the
661 Yellow River basin, China, *J. Hydrol.*, 584, 124751,
662 <https://doi.org/10.1016/j.jhydrol.2020.124751>, 2020.
- 663 Wang, X., Luo, P., Zheng, Y., Duan, W., Wang, S., Zhu, W., Zhang, Y., and Nover, D.: Drought
664 Disasters in China from 1991 to 2018: Analysis of Spatiotemporal Trends and Characteristics,
665 *Remote Sens.*, 15, 1708, <https://doi.org/10.3390/rs15061708>, 2023.
- 666 Wang, Z., Zhong, R., Lai, C., Zeng, Z., Lian, Y., and Bai, X.: Climate change enhances the severity
667 and variability of drought in the Pearl River Basin in South China in the 21st century, *Agric. For.
668 Meteorol.*, 249, 149-162, <https://doi.org/10.1016/j.agrformet.2017.12.077>, 2018.
- 669 Wei, H., Liu, X., Hua, W., Zhang, W., Ji, C., and Han, S.: Copula-Based Joint Drought Index Using
670 Precipitation, NDVI, and Runoff and Its Application in the Yangtze River Basin, China, *Remote
671 Sens.*, 15, 4484, <https://doi.org/10.3390/rs15184484>, 2023.
- 672 Wen, X., Tu, Y., Tan, Q., Li, W., Fang, G., Ding, Z., and Wang, Z.: Construction of 3D drought
673 structures of meteorological drought events and their spatio-temporal evolution characteristics, *J.
674 Hydrol.*, 590, 125539, <https://doi.org/10.1016/j.jhydrol.2020.125539>, 2020.
- 675 Wilhite, D.A., and Glantz, M.H.: Understanding: the drought phenomenon: the role of definitions,
676 *Water Int.*, 10, 111-120, 1985.
- 677 Won J, Choi J, Lee O, and Kim, S.: Copula-based Joint Drought Index using SPI and EDDI and its
678 application to climate change, *Sci. Total Environ.*, 744, 140701,
679 <https://doi.org/10.1016/j.scitotenv.2020.140701>, 2020.



- 680 Xu, H., Wang, X., Zhao, C., and Yang, X.: Diverse responses of vegetation growth to meteorological
681 drought across climate zones and land biomes in northern China from 1981 to 2014, *Agric. For.*
682 *Meteorol.*, 262, 1-13, <https://doi.org/10.1016/j.agrformet.2018.06.027>, 2018.
- 683 Xu, Y., Zhang, X., Hao, Z., Singh, V.P., and Hao, F.: Characterization of agricultural drought
684 propagation over China based on bivariate probabilistic quantification, *J. Hydrol.*, 598, 126194,
685 <https://doi.org/10.1016/j.jhydrol.2021.126194>, 2021.
- 686 Xu, Y., Zhang, X., Wang, X., Hao, Z., Singh, V.P., and Hao, F.: Propagation from meteorological
687 drought to hydrological drought under the impact of human activities: A case study in northern
688 China, *J. Hydrol.*, 579, 124147, <https://doi.org/10.1016/j.jhydrol.2019.124147>, 2019.
- 689 Yang, J., Gong, D., Wang, W., Hu, M., and Mao, R.: Extreme drought event of 2009/2010 over
690 southwestern China, *Meteorol. Atmos. Phys.*, 115, 173-184, [https://doi.org/10.1007/s00703-011-](https://doi.org/10.1007/s00703-011-0172-6)
691 [0172-6](https://doi.org/10.1007/s00703-011-0172-6), 2012.
- 692 You, M., He, Z.H., Zhang, L., Yang, M.K., and Pi, G.N.: Characteristics of agricultural and
693 meteorological drought in Guizhou Province and their response relationship, *J. Soil Water*
694 *Conserv.*, 36, 255-264, 2022.
- 695 Zhang, F., Biederman, J.A., Dannenberg, M.P., Yan, D., Reed, S.C., and Smith, W.K.: Five decades
696 of observed daily precipitation reveal longer and more variable drought events across much of
697 the western United States, *Geophys. Res. Lett.*, 48, e2020GL092293,
698 <https://doi.org/10.1029/2020GL092293>, 2021.
- 699 Zhang, J., Wang, J., Chen, S., Wang, M., Tang, S., and Zhao, W.: Integrated Risk Assessment of
700 Agricultural Drought Disasters in the Major Grain-Producing Areas of Jilin Province, China,
701 *Land.*, 12, 160, <https://doi.org/10.3390/land12010160>, 2023.



- 702 Zhang, T., Su, X., Zhang, G., Wu, H., Wang, G., and Chu, J.: Evaluation of the impacts of human
703 activities on propagation from meteorological drought to hydrological drought in the Weihe River
704 Basin, China, *Sci. Total Environ.*, 819, 153030, <https://doi.org/10.1016/j.scitotenv.2022.153030>,
705 2022.
- 706 Zhang, X., Hao, Z., Singh, V.P., Zhang, Y., Feng, S., Xu, Y., and Hao, F.: Drought propagation under
707 global warming: Characteristics, approaches, processes, and controlling factors, *Sci. Total*
708 *Environ.*, 838, 156021, <https://doi.org/10.1016/j.scitotenv.2022.156021>, 2022.
- 709 Zhang, Y., Hao, Z., Feng, S., Zhang, X., Xu, Y., and Hao, F.: Agricultural drought prediction in
710 China based on drought propagation and large-scale drivers, *Agric. Water Manage.*, 255, 107028,
711 <https://doi.org/10.1016/j.agwat.2021.107028>, 2021.
- 712 Zhang, Y., Huang, S., Huang, Q., Leng, G., Wang, H., and Wang, L.: Assessment of drought
713 evolution characteristics based on a nonparametric and trivariate integrated drought index, *J.*
714 *Hydrol.*, 579, 124230, <https://doi.org/10.1016/j.jhydrol.2019.124230>, 2019.
- 715